Journal of Materials Chemistry A

Accepted Manuscript

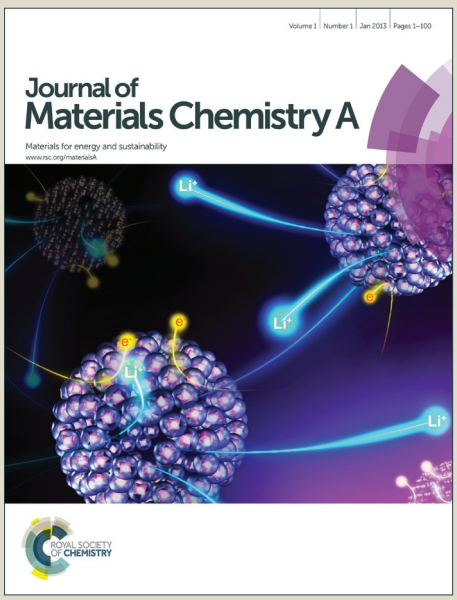

ROYAL SOCIETY OF CHEMISTRY

www.rsc.org/materialsA

Cite this: DOI: 10.1039/c0xx00000x

www.rsc.org/xxxxxx

ARTICLE TYPE

Oxygen Reduction in the Nanocage of Metal-Organic Frameworks with An Electron Transfer Mediator

Min Jiang[1a], Liangjun Li[1a], Dandan Zhu[a], Hongyu Zhang[b]* and Xuebo Zhao[a]*

Received (in XXX, XXX) Xth XXXXXXXXX 20XX, Accepted Xth XXXXXXXXX 20XX

DOI: 10.1039/b000000x

A highly porous metal-organic framework (MOF) containing copper metal centres and nanocages was modified onto a glassy carbon electrode as a noble-metal-free electrocatalyst for oxygen reduction reaction. The nanocages in metal-organic framework were fully activated by solvent-exchange method. Although both of the as-prepared MOF and the activated MOF samples showed the electrochemical activity of Cu^{2+}/Cu^{+} redox pairs by cyclic voltammetric studies, only the activated MOF samples could catalyze oxygen reduction reaction. In order to avoid detachment of the activated sample from the glassy carbon electrodes surface owing to low-effective electron-transfer pathway during electrochemical scanning in aqueous solution, reduced graphene oxide (RGO) were immobilized onto glassy carbon electrode surface as an binder and electron transfer mediator under MOF active layer. The MOF layer on RGO immobilized glassy carbon electrode can catalyze the oxygen reduction reaction through a 2-4 electrons reduction pathway. Furthermore, the occurrence potential of ORR versus Ag/AgCl by MOF catalyst shifted to the positive near 100 mV in comparison with other MOF catalysts.

Introduction

As one of crystalline porous materials, metal-organic frameworks (MOFs) have attracted considerable attention for their potentially valuable applications in the field of gas storage and catalysis.[1-3] On one hand, pore size and micropore volume of MOF are critical for their gas storage capacity and gas separation properties.[4] On the other hand, the metal content of inorganic nodes in MOFs offering active sites plays an important role in determining their catalytic performance.[3, 5] Combination of the porosity and catalytic feature for gas molecules could urge MOFs to be involved in efficient, clean energy storage and conversion, especially electrochemistry field.[6, 7] Oxygen reduction reaction (ORR) is a fundamental reaction in energy converting systems such as fuel cell,[8-11] where oxygen and hydrogen are forming water by a direct four-electron reduction pathway at the cathode. The critical challenge for improving fuel cells is making advancement in the catalyst for ORR to increase the catalytic efficiency. In this case, as a non-noble metal material, MOF is expected to act as an oxygen container and an ORR catalyst simultaneously. The investigation of MOFs in the electrocatalytic field is quite current and gradually expanding.[6, 12-19] Although some reports focused on the use of MOF as a sacrificial precursor for preparing ORR catalysts,[20-25] only few examples of the preserved MOFs structures have been reported for ORR electrocatalysis.[26, 27] Jahan et al. synthesized a composite graphene/Fe-porphyrin MOF which exhibited enhanced electrocatalytic activity towards the ORR in alkaline medium with an appropriate amount of functionalized graphene building blocks added.[27] The hybrid catalyst exhibited ORR at -0.23V versus Ag/AgCl. Another example for ORR is displayed by the classical MOF compound Cu-BTC and Cu-bipy-BTC with bipy as an auxiliary ligand.[26] The author demonstrated that Cu-bipy-BTC was more stable in aqueous media than Cu-BTC and it exhibited a stable electrocatalytic activity towards four-electron reduction of O_2. In contrast to the richness and variety of MOF structures, unfortunately, only sporadic MOFs have been reported for the application of ORR. The possible reasons are proposed as follows: (1) the instability of MOF structure in aqueous medium; (2) the poor contacts between micro-sized MOF and the electrode surface, (3) a lack of knowledge on the correlation between MOF structure feature and electrochemical performance. Actually, because some functional groups in framework prefer to form favourable interaction with gas molecues[28], taking knowledge of the relevance of oxygen storage behavior in pores to electrocatalysis behavior of porous materials will benefit the design and selection of MOF electrocatalyst for the purpose of electrocatalytic ORR.

A novel MOF compound (NPC-4, NPC: Nanoporous cage) containing copper with nanocage structure was synthesized recently by our group.[29] By activating nanocages of MOF by solvent-exchange method, this MOF compound possessed high storage capacity towards hydrogen, carbon dioxide and methane besides oxygen. It is attractive to consider whether the activated MOFs sample is optimal choice for the investigation on the electrochemical property of MOFs or not. To our knowledge, no research on this issue has been reported to date. In this paper, we

aim to take knowledge of the relevance of the electrochemical property and the activated pores in MOFs for the applications of MOFs as the catalysts in various electrochemical reactions. In addition, considering the general poor contacts between micro-sized MOF and the smooth electrode surface, reduced graphene oxide (RGO)[30] which is a good charge-carrier, is expected to act as an electron transfer mediator and binder between MOF active layer and electrode to enhance the stability of electrochemical performance and facilitate the electrocatalytic role of MOF for ORR. This promising strategy can be applied for the immobilization of MOFs on electrode surface for various electrocatalytic reactions.

Experimental procedure

Materials

Graphite was purchased from Sigma-Aldrich. 5% Nafion solution (5 wt%) was obtained from Aldrich. All other chemicals were of analytic grade. All solutions were prepared by using Milli-Q water.

MOF synthesis

This NPC-4 MOF compound $Cu_2(TMBDI)(H_2O)_2$ (where TMBDI=2,3,5,6-tetramethyl-benzene-1,4-di-isophalate) was synthesized according to the recent report.[29] Briefly, NPC-4 crystal was obtained by solvent thermal reaction at 373 K for 72 hours of $Cu(NO_3)_2$ and TMBDI in a solvent of N,N-Dimethylacetamide (DMA)/H_2O (volume fraction 3:1) with a few HNO_3 addition. All bulk crystals need to be ground in agate mortar by hands before being modified onto electrode.

RGO synthesis

Graphene oxide (GO) was synthesized from natural graphite powder following Hummers method.[31] Reduced graphene oxide (RGO) sheets were prepared according to the similar procedure reported in literature.[32] In brief, 0.1 g GO was dispersed in 20 mL water and to the dispersion was added 0.2 g $NaBH_4$. The mixture was allowed to stir for 20 min and then heated in a steam bath for 3 h. The isolation of as-made RGO was operated by centrifugation, good washing with water and acetone, and drying.

Instruments

Gas adsorption isotherms were conducted on IGA gravimetric analyser (Hiden Isochema, IGA-001, Warrington, UK). Fourier transform infrared (IR) measurements were performed on a Nicolet 6700 FTIR spectrometer. Powder X-ray diffraction (PXRD) was carried out with a BRUKER D8-Focus Bragg-Brentano X-ray Powder Diffractometer equipped with a Cu kα radiation (λ = 0.154 nm). Atomic force microscopy (AFM) images were recorded by using Agilent 5400 AFM. Scanning Electron Microscopy (SEM) images were obtained with a Hitachi S-4800 (Japan) scanning electron microscope at an acceleration voltage of 5 kV. Cyclic voltammetry was carried out on a computer-controlled electrochemical analyzer (CHI 660D, China). Rotating disk electrode (RDE) experiments were carried out on a RRDE-3A (ALS Co., Ltd) and CHI electrochemical workstation (CHI 660D, China). All cyclic voltammeters measurements were carried out using a three-electrode system with glassy carbon electrode (GCE) as working electrode, Pt wire as counter electrode, and Ag/AgCl (KCl-saturated) as reference electrode. Linear sweep voltametry (LSV) was performed at a glassy carbon RDE working electrode with a 3-mm diameter, a platinum wire counter electrode, and a Ag/AgCl (KCl-saturated) reference electrode.

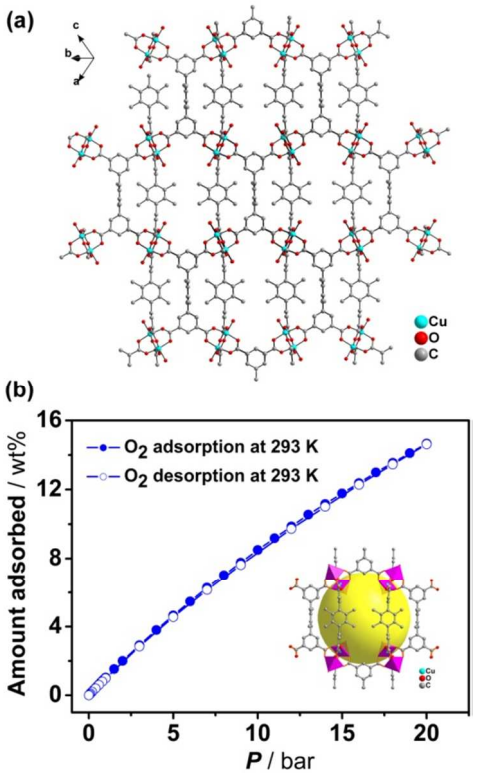

Fig. 1 (a) Crystal structure of NPC-4. Coordination framework is shown as ball-and-stick model. (b) O_2 sorption isotherm at 293K. The inset is ball-and-stick model representation of nanocage in NPC-4. Coordination of active center Cu is present by purple polyhedron.

Modification of working electrode

Prior to use, a GCE working electrode was polished mechanically with alumina slurry and then washed with Milli-Q water and ethanol and allowed to dry. To avoid the disturbance of GCE substrates in XRD characterization, Ti electrode was used for XRD measurements. Prior to use, Ti electrode (1 cm×1 cm plate) was immersed into 10% hot NaOH solution for 30 min to remove surface grease stains, and then put into the mixture solution of HF: HNO_3: H_2O (volume ratio 1:3:80) for 30 min to remove the oxide layer. Finanlly Ti electrode was washed with Milli-Q water and dried.

To prepare NPC-4 modified electrodes, 2 mg of the as-prepared samples was dispersed into 1 mL 0.05% Nafion solution to give homogeneous suspension upon bath sonication. A 5 μL of the suspension was dip-coated onto a GCE, a RGO modified GCE or Ti electrode and dried at ambient temperature for 24 h. RGO aqueous dispersion solution was obtained by dispersing 1mg RGO into 5mL water upon bath sonication. A 5 μL of RGO suspension was dip-coated onto GCE and dried at ambient temperature for 24 h to give a RGO immobilized GCE. All electrochemical experiments were performed at room temperature.

Results and discussions

Nanocages of MOF for oxygen storage

As shown in Fig.1a, methyl functionalized carboxylate ligands and the di-copper paddle-wheel secondary building units (SBUs) are assembled in a special way to form a three-dimensional porous network NPC-4. The network can be viewed as a connection of many closely arranged nano-scale polyhedron cages whose diameter is around 1.6 nm. Moreover, the nanocage in NPC-4 framework has windows of diameter ~ 0.6 nm which is large enough to enable gas molecule to pass through. Fig.1b provides the oxygen sorption measurement of NPC-4 at 293K. This typical isotherm indicates the microporous characteristic of NPC-4 and its Langmuir surface area is 2130 m^2/g. Such highly regular nanoporous structures and high density of open metal sites enable this material with high gas storage capacity. In the published results, the adsorption of oxygen molecules by microporous materials typically originated from the existence of some interactions between the surface of the pores and the oxygen molecules and of the fact that they are in an unusual state arising from an electronic effect and a confinement effect.[28] From the single fragment of the 3D polyhedron cages shown in the inset of Fig.1b, it is observed that the open metal sites of Cu are in the inner surface of nanocage represented by the large yellow sphere. Hence, the exposure of active sites to the oxygen molecules in nanocage will facilitate further reduction of oxygen.

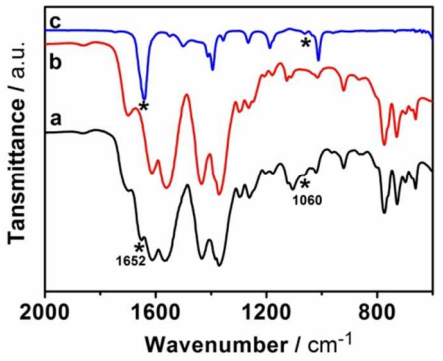

Fig. 2 IR spectra of as-made NPC-4 (a), activated NPC-4 (b) in KBr pellet and DMA solvent (c) in silicon slide.

Prior to the gas sorption measurement, a necessary activation process must be operated by removing guest molecules from nanocage in order to take up various target gases in nanocage of MOF.[33] As for as-prepared NPC-4 crystal, two and a half N,N-dimethylacetamide (DMA) molecules and four water molecules have been proved to be involved in the nanocage on the basis of single crystal X-ray diffraction, thermal gravity analysis and elemental analysis.[29] Therefore, the activation procedure includes two steps. First step is the immersion of the sample in acetone for seven days and refreshing acetone daily to completely extract DMA molecules encapsulated in nanocage. Secondly, the sample was dried at 393K under vacuum for one hour to remove acetone and water molecules from nanocage and finally the fully activated MOFs were provided. The recent results concluded from the pore volume, void space ratio and thermogravimetric analysis illustrated that the activation process did not cause the network collapse of NPC-4 crystal.[29]

Infrared spectroscopy is utilized to verify the solvent exchange procedure. In the IR spectrum of as-prepared NPC-4 (curve *a* in Fig.2), the characteristic peaks at about 1652 cm^{-1} and 1060 cm^{-1} are assigned to the stretching vibration of C=O in amido bond and C-N bond in DMA solvent species (curve *c* in Fig.2), respectively. When DMA molecules are replaced by solvent exchange way, the vibration of amido bond in the IR spectra disappears as shown in curve *b* of Fig.2, It indicates that DMA molecules have been fully removed and nanocages were completely activitated.

Electrochemical performance of two MOFs

As-prepared NPC-4 and the activated NPC-4 samples were modified onto GCE and their electrochemical behaviours were performed in 0.1 mol/L phosphate buffer (pH 6.0) solution by cyclic voltammetry (CV), respectively. From Fig.3a, it is obviously seen that as-prepared NPC-4 sample shows an electrochemical activity with the appearance of a pair of redox waves. The redox wave corresponds to Cu^{2+}/Cu^{+} reversible state,[34] where the cathodic wave is a prominent peak while the anodic wave is a wide peak. Such an electrochemical performance of NPC-4 modified onto GCE is very stable without decaying after tens of CV cycles. In general, micro-sized MOF sample provided by manual grind has poor adhesion to the smooth electrode surface in nanoscale, although small amount of Nafion was added. But non-activated sample still keep the stability of adhesion without the ingress of electrolyte ions into nanocage. Its electrochemical activity mainly depends on the electron transport between electrode and a few outer metal ions near electrode surface other than inner metal open sites. In contrast with zeolites and other microporous aluminosilicates, the order porosity of MOFs is responsible for significant redox conductivity.[7] However, full occupancy of DMA molecules reduces the redox conductivity of as-prepared NPC-4 sample, which causes the irreverability of redox peaks.

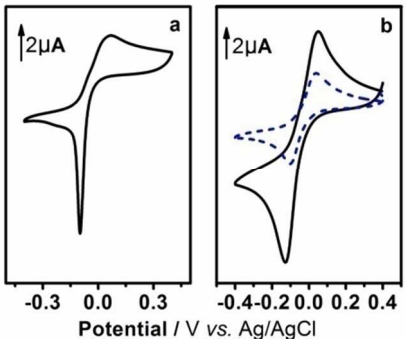

Fig. 3 CVs of as-prepared NPC-4 (a) and activated NPC-4 (b) modified onto the GCE in 0.1 mol/L phosphate buffer (pH 6.0) solution. Dash line represents CV of activated NPC-4 after tens of CV cycles. Scan rate: 20 mV/s.

When the nanocages of NPC-4 were activated by removing solvent molecules, the electrochemical reversibility of sample had been improved owing to the increased redox conductivity (solid curve in Fig.3b). There is few difference in the potential of redox peak pairs comparing with as-prepared sample. Unfortunately, the activated NPC-4 modified layer was not stable enough during

electrochemical scanning so that the current weakened about two third after tens of CV cycles (dash curve in Fig.3b). It is because that the ingress/issue of electrolyte ions in/from the MOF lattice causes the rapid extension of the electron transport and hopping between adjacent metal ions along the entire crystal.[35] Such a change strongly weakens the electron transport across electrode/crystal interface on the basis of the poor connection between them. Hence, this incompatibility between an increasing flexibility of MOF lattice with free electron mobility and a low-effective electron transport from electrodes resulted in some loss of MOF sample modified on GCE.

Electrocatalytic behaviors of two MOFs towards ORR

The electrocatalytic activity of NPC-4 towards ORR was evaluated in 0.1 mol/L phosphate buffer (pH 6.0) solution. Fig.4 shows the voltammograms of as-prepared and activated NPC-4 samples modified onto GCE in a N_2- and O_2-saturated solution in the potential range from -0.4 V to 0.4 V. One can see that the presence of O_2 into the electrolyte solution does not affect the currents of reduction peak and oxide peak in Fig.4a. It demonstrates that as-prepared sample could not catalyze the electrochemical reduction of oxygen molecules. The increased reduction current occurred at -0.4 V is contributed by the response of GCE itself towards ORR. When the NPC-4 was activated after acetone-exchange ways, the modified GCE began to response to the electrochemical reduction of oxygen (as shown in Fig.4b). The cathode peak current at -0.13 V clearly increases while the reversed anode peak current at 0.05V decreases as the electrolyte solution is saturated with O_2. At the bare GCE, ORR happened on the potential of -0.3 V (the inset of Fig.4b). By contrast, the potential of oxygen reduction on activated NPC-4 modified GCE is -0.13 V showing a positive shift of the potential. It suggests that the activated NPC-4 possess electrocatalytic activity towards ORR. Furthermore, the reduction of oxygen begins at the same potential of the reduction of Cu^{2+}, and this fact supports that the oxygen reduction is catalyzed by Cu^{+}. Simultaneously, the catalytic center Cu^{+} ion is returned to Cu^{2+} ion by oxygen. In comparison with graphene/Fe-porphyrin MOF[27] and Cu-bipy-BTC[26], the occurrence potential of ORR versus Ag/AgCl by NPC-4 catalyst shifted to the positive near100 mV.

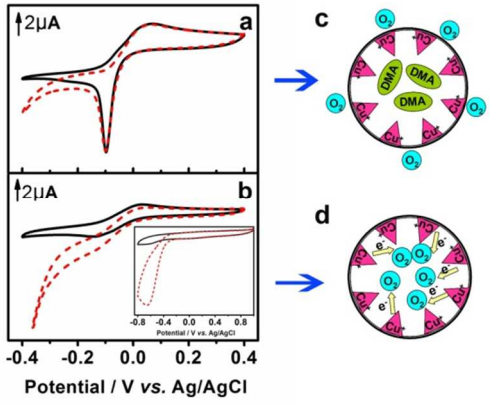

Fig. 4 CVs of as-prepared NPC-4 (a) and activated NPC-4 (b) modified onto the GCE in 0.1 mol/L phosphate buffer (pH 6.0) solution saturated with N_2 (solid curves) and O_2 (dot curves). The inset represents the CVs obtained at bare GCE. Scan rate: 20 mV s^{-1}. Corresponding schematics for the electrochemical reduction of O_2 by the catalytic role of as-prepared NPC-4 (c) and activated NPC-4 (d).

Such results of electrocatalytic reduction of oxygen triggered by activating the nanocages can be tentatively explained by the following reasons. Because the oxygen reduction is catalyzed by Cu^{+} and the reduction of Cu^{2+} to Cu^{+} was performed in the nanocage of NPC-4, the precondition for oxygen reduction is O_2 being encapsulated in the nanocage. As for as-prepared NPC-4 sample, the occupancy of nanocage by DMA molecules can hinder the diffusion of dissolved oxygen in electrolyte solution into nanocage, which results in no electrocatalytic response to the oxygen reduction (see Fig.4c). With the enlargement of free space in nanocage by removing the DMA molecules, dissolved oxygen molecules can enter into nanocage and was electrocatalytically reduced by Cu^{+} (see Fig.4d).

Electrocatalytical stability of activated MOF layer

Stability in the electrochemical process is a very important parameter for the application of electrocatalyst. XRD can provide direct evidence for monitoring stability of MOF structure during electrocatalytical process. Fig.5 exhibits XRD patterns of

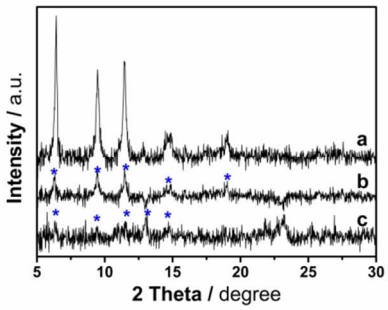

Fig. 5 XRD patterns of as-made activated NPC-4 on Ti electrode (a), activated NPC-4 on Ti electrode after ten electrocatalytical cycles for ORR (b), and activated NPC-4 on Ti electrode after twenty electrocatalytical cycles for ORR (c).

activated NPC-4 sample on Ti electrode during electrocatalytical ORR. Curve *a* displayed very good diffraction pattern of crystalline NPC-4 on Ti electrode. After the modified Ti electrode was operated in electrocatalytical ORR for ten cycles, crystallinity of NPC-4 was partly kept while the diffraction pattern obviously weakened as shown in Curve *b*. After the application in twenty electrocatalytical cycles for ORR, activated NPC-4 modified on Ti electrode showed very weak diffraction as shown in Curve *c*. Although part samples were considered to detach from Ti electrode surface because of weak interaction with Ti electrode, the gradual disappearance of diffraction pattern was mainly caused by network collapse of crystalline NPC-4. These results demonstrated activated NPC-4 layer was stable in a limited period for ORR and longer-period application for ORR caused the network collapse of crystalline NPC-4. The main reason may be that consecutive electron-transfer from catalytic center Cu^{+} to oxygen molecule weakens the stability of coordination polyhedron in SBUs and induces the network collapse of the whole crystalline NPC-4. Although details about collapsed species were unknown, they still showed weak electrocatalytical signal toward ORR owing to the existence of residual di-copper paddle-wheel SBUs.

SEM technology was also applied to investigate the stability of

activated NPC-4 layer on GCE. It was seen that some activated NPC-4 aggregated on GCE surface in Fig.6a. From the SEM image of single crystalline NPC-4, the order laminar structure was observable in Fig.6b. Because the sample was treated by grind and ultrasonication, activated NPC-4 did not show perfect crystallinity as as-synthesized single crystal. After the application in ten electrocatalytical cycles for ORR, rod-like structures began to appear and coexisted with crystalline NPC-4 as shown in Fig.6c. Such rod-like structure with 50 percent occupancy was regarded as the collapsed products of laminar NPC-4 crystals. More CV scans for ORR caused the large-scale collapse of order laminar structure, as shown in Fig.6d. These results are consistence with the above conclusions from XRD.

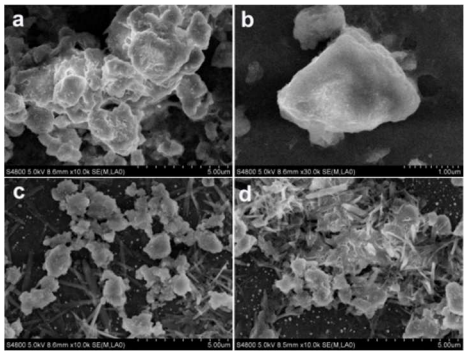

Fig. 6 SEM images of as-made activated NPC-4 on GCE (a) and (b), activated NPC-4 on GCE after ten electrocatalytical cycles for ORR (c), activated NPC-4 on GCE after twenty electrocatalytical cycles for ORR (d).

In view of the structural changes of activated NPC-4 on GCE during electrocatalytical ORR, all data and discussions were based on activated NPC-4 sample with mostly preserved network structure on GCE during electrocatalytical process.

RGO modified layer on GCE

Although the electrocatalytic behaviour of activated NPC-4 sample towards ORR is visible, the detachment of NPC-4 modified layer on GCE limits its application. In order to satisfy the exertion of NPC-4 for electrocatalytic ORR, it was considered to modify RGO onto GCE surface under MOF active layer. On one hand, besides large specific surface area, the grafold and dense exposed edges of RGO could provide more contact points for the adhesion of MOF than bare GCE.[36, 37] On the other hand, the highly electric conductivity of RGO could significantly facilitate the electron transport between MOF layer and electrode. In view of the above two aspects, introduction of RGO was expected to provide more pathways for highly effective electron transport from electrode to MOF layer and ensure the expression of electrocatalytical role of MOF toward ORR.

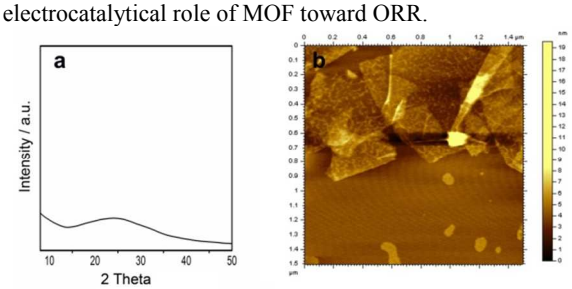

Fig. 7 XRD patterns of reduced graphene oxide (a) and AFM image of reduced graphene oxide sanple prepared by drop-casting RGO aqueous dispersion onto mica sheet (b).

The obtained RGO is characterized by the powder X-ray diffraction. As shown in Fig.7a, the XRD pattern of RGO exhibits a typical broad peak around 24°. The dispersion of RGO in water was drop-cast onto mica and one single sheet of RGO is obvious observed from AFM image as shown in Fig.7b. The average thickness of as-prepared RGO is about 1.0 nm.

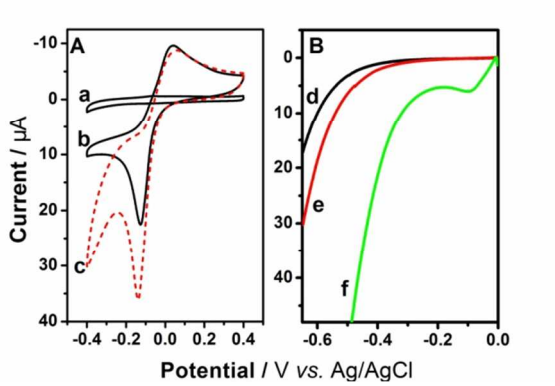

Fig. 8 (A) CVs of RGO immobilized GCE (a) and activated NPC-4 modified RGO/GCE (b) in N_2-saturated 0.1 mol/L phosphate buffer (pH 6.0) solution. Curve *c* represents CV of activated NPC-4 modified RGO/GCE in O_2-saturated 0.1 mol/L phosphate buffer (pH 6.0) solution. Scan rate: 20 mV/s. (B) LSVs of bare RDE (d), RGO immobilized RDE (e) and NPC-4 modified RGO/RDE (f) in O_2-saturated 0.1 mol/L phosphate buffer (pH 6.0) solution. Electrode rotation rate: 1600 rpm. Scan rate: 2 mV/s.

Electrocatalytic behaviors of MOFs modified RGO/GCE towards ORR

RGO itself did not show any redox response in the potential range from -0.4V to 0.4V when it was modified onto GCE surface (as curve *a* in Fig.8A). When the activated NPC-4 was modified onto RGO/GCE surface, its CV curve exhibited well-defined redox peaks as shown curve *b* in Fig.8A. Moreover, its electrochemical response seemed very stable without peak shrinking after tens of CV scans. When the electrolyte solution was saturated with O_2, the activated NPC-4 modified RGO/GCE performed observable electrocatalytic response at -0.13V (as curve *c* in Fig.8A). In order to make clear the electrocatalytic behaviour of multi-composite electrode for ORR, the linear sweep voltametries were operated on bare GCE (curve *d* in Fig.8B), RGO modified GCE (curve *e* in Fig.8B) and NPC-4 modified RGO/GCE (curve *f* in Fig.8B) in a solution saturated with O_2 in the same condition, respectively. By comparing curve *d*, *e* and *f*, it further proves that NPC-4 plays a main role in catalyzing ORR on the potential of -0.13 V. However, the coexistence of RGO with NPC-4 exactly enhanced the adhesion stability of MOF electrocatalyst upon retaining the catalytic activity for ORR. As expected, the fast electron mobility of graphene and its unique surface properties facilitated and accelerated the electron transfer between GCE and NPC-4 immobolized sample through highly electrically conductive RGO channels. Such a fast electron transfer route across electrode/crystal interface can resist the detachment of active NPC-4 layer from GCE surface caused by the extended redox conductivity along the whole MOF lattice.

A more detailed analysis of the oxygen reduction properties of NPC-4/RGO catalysts has been carried out by RDE measurements. Fig.9 shows typical RDE curves obtained at

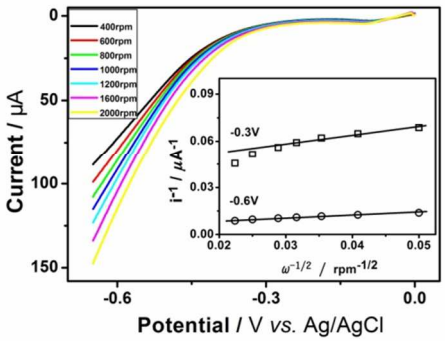

Fig. 9 RDE linear sweep voltammograms of activated NPC-4 in O_2-saturated 0.1 mol/L phosphate buffer (pH 6.0) solution with various rotation rates at a scan rate of 2 mV/s. Inset is Koutecky−Levich plots of activated NPC-4 at different electrode potentials.

different rotation rates. Koutecky–Levich plots,[9] the inset of Fig.9, is obtained as a linear fit of the data taken from the corresponding polarization curves (Fig.9) by applying reported values for oxygen solubility oxygen diffusivity ($D=1.4\times10^{-5}$ cm^2/s) and the kinematic viscosity of 0.1 mol/L PBS electrolyte ($\nu=0.01$ cm^2/s) to 0.62 $nFAD^{2/3}\nu^{-1/6}C_{O2}$ equation.[38] From the slope of Koutecky–Levich plots at -0.3 V and -0.6 V, B factor was estimated to be 3.3 $\mu A\cdot rpm^{-1/2}$ and 5.9 $\mu A\cdot rpm^{-1/2}$, respectively. According to the value of B, the number of electrons transferred during the reduction of an oxygen molecule is about 1.8 electrons at -0.3 V and 3.2 electrons at -0.6 V. At a potential of -0.3 V, ORR occurs via the near 2-electron reduction pathway where it is reduced to hydrogen peroxide. At a potential of -0.6 V, ORR is regarded to proceed via almost 4-electron reduction pathway where it is reduced to H_2O. This result shows that the stably attached MOF layer on RGO immobilized glassy carbon electrode can catalyze the oxygen reduction reaction through a 2-4 electrons reduction pathway depending on the overpotential.

Conclusions

This work demonstrates the first example of the electrocatalytic reduction of oxygen triggered by solvent-exchange method in the nanocage of highly porous metal-organic framework. Solvent-exchange procedure activates the nanocage, and the reduction of oxygen exactly occurred in the nanocage. Introduction of reduced grahene oxide immobilized glassy carbon electrode under NPC-4 active layer provide more contact points for the adhesion of NPC-4 than bare GCE, in other words, more effective pathways for electron transport from electrode to NPC-4 layer. The electrochemical stability of NPC-4 layer was enhanced to large extent and the detachment of activated NPC-4 sample from glassy carbon electrode surface was effectively avoided. Moreover, NPC-4/RGO catalyst exhibits a more positive ORR onset potential at −0.13 V vs Ag/AgCl (KCl-saturated) than other reported MOF electrocatalysts, and it can catalyze the oxygen reduction reaction through a 2-4 electrons reduction pathway depending on the overpotential. This strategy of the catalysis triggered by solvent-exchange way and the usage of RGO mediator can offer researchers a new direction to develop MOF as electrocatalysts in many fields.

This work was financially supported by National Natural Science Foundation of China (Grant no. 21173246 and 21103215) and the "Hundred-talent Project" (KJCX2-YW-W34) of the Chinese Academy of Sciences.

Notes and references

[a] *Energy Utilization Technology Center, Qingdao Institute of Bioenergy and Bioprocess Technology, Chinese Academy of Sciences, No.189 Songling Road, Qingdao, 266101, P. R. China. Fax: +86-532-80662728; Tel: +86-532-80662729; E-mail: zhaoxb@qibebt.ac.cn*
[b] *College of Chemistry and Chemical Engineering, Ocean University of China, Qingdao 266100, P. R. China. E-mail: hongyuzhang@ouc.edu.cn*
[1] *These authors contributed equally to this work.*

1. K. Sumida, D. L. Rogow, J. A. Mason, T. M. McDonald, E. D. Bloch, Z. R. Herm, T.-H. Bae and J. R. Long, *Chem. Rev.*, 2012, **112**, 724-781.
2. F. Vermoortele, M. Vandichel, B. Van de Voorde, R. Ameloot, M. Waroquier, V. Van Speybroeck and D. E. De Vos, *Angew. Chem. Int. Ed.*, 2012, **51**, 4887-4890.
3. J. Lee, O. K. Farha, J. Roberts, K. A. Scheidt, S. T. Nguyen and J. T. Hupp, *Chem. Soc. Rev.*, 2009, **38**, 1450-1459.
4. H. Zhao, Z. Jin, H. Su, J. Zhang, X. Yao, H. Zhao and G. Zhu, *Chem. Commun.*, 2013, **49**, 2780-2782.
5. A. Dhakshinamoorthy, M. Alvaro and H. Garcia, *Catal. Sci. Technol.*, 2011, **1**, 856-867.
6. A. Morozan and F. Jaouen, *Energ. Environ. Sci.*, 2012, **5**, 9269-9290.
7. A. Doménech-Carbó, in *Electrochemistry of Porous Materials*, Taylor & Francis, London, 2009, pp. 95-115.
8. Z. Peng, S. A. Freunberger, L. J. Hardwick, Y. Chen, V. Giordani, F. Bardé, P. Novák, D. Graham, J.-M. Tarascon and P. G. Bruce, *Angew. Chem. Int. Ed.*, 2011, **50**, 6351-6355.
9. S. Strbac, *Electrochim. Acta*, 2011, **56**, 1597-1604.
10. Y.-C. Lu, H. A. Gasteiger and Y. Shao-Horn, *J. Am. Chem. Soc.*, 2011, **133**, 19048-19051.
11. A. H. C. Sirk, S. A. Campbell and V. I. Birss, *J. Electrochem. Soc.*, 2008, **155**, B592-B601.
12. Z. D. Chang, N. S. Gao, Y. J. Li and X. W. He, *Anal. Mathods*, 2012, **4**, 4037-4041.
13. B. Nohra, H. El Moll, L. M. R. Albelo, P. Mialane, J. Marrot, C. Mellot-Draznieks, M. O'Keeffe, R. N. Biboum, J. Lemaire, B. Keita, L. Nadjo and A. Dolbecq, *J. Am. Chem. Soc.*, 2011, **133**, 13363-13374.
14. R. S. Kumar, S. S. Kumar and M. A. Kulandainathan, *Electrochem. Commun.*, 2012, **25**, 70-73.
15. L. Yang, S. Kinoshita, T. Yamada, S. Kanda, H. Kitagawa, M. Tokunaga, T. Ishimoto, T. Ogura, R. Nagumo, A. Miyamoto and M. Koyama, *Angew. Chem. Int. Ed.*, 2010, **49**, 5348-5351.
16. K. F. Babu, M. A. Kulandainathan, I. Katsounaros, L. Rassaei, A. D. Burrows, P. R. Raithby and F. Marken, *Electrochem. Commun.*, 2010, **12**, 632-635.
17. H. Hosseini, H. Ahmar, A. Dehghani, A. Bagheri, A. Tadjarodi and A. R. Fakhari, *Biosens. Bioelectron.*, 2013, **42**, 426-429.
18. Y. Gong, T. Wu, P. G. Jiang, J. H. Lin and Y. X. Yang, *Inorg. Chem.*, 2013, **52**, 777-784.

19. J. Song, Z. Luo, D. K. Britt, H. Furukawa, O. M. Yaghi, K. I. Hardcastle and C. L. Hill, *J. Am. Chem. Soc.*, 2011, **133**, 16839-16846.
20. Q. Li, P. Xu, W. Gao, S. Ma, G. Zhang, R. Cao, J. Cho, H.-L. Wang and G. Wu, *Adv. Mater.*, 2013, DOI: 10.1002/adma.201304218..
21. S. Q. Ma, G. A. Goenaga, A. V. Call and D. J. Liu, *Chem. Eur. J.,* 2011, **17**, 2063-2067.
22. E. Proietti, F. Jaouen, M. Lefevre, N. Larouche, J. Tian, J. Herranz and J. P. Dodelet, *Nat. Commun.*, 2011, **2**, 416-417.
23. J. Tian, A. Morozan, M. T. Sougrati, M. Lefevre, R. Chenitz, J. P. Dodelet, D. Jones and F. Jaouen, *Angew. Chem. Int. Ed.*, 2013, **52**, 6867-6870.
24. T. Palaniselvam, B. P. Biswal, R. Banerjee and S. Kurungot, *Chem. Eur. J.,* 2013, **19**, 9335-9342.
25. W. Chaikittisilp, K. Ariga and Y. Yamauchi, *J. Mater. Chem. A*, 2013, **1**, 14-19.
26. J. Mao, L. Yang, P. Yu, X. Wei and L. Mao, *Electrochem. Commun.*, 2012, **19**, 29-31.
27. M. Jahan, Q. Bao and K. P. Loh, *J. Am. Chem. Soc.*, 2012, **134**, 6707-6713.
28. S. Shimomura, M. Higuchi, R. Matsuda, K. Yoneda, Y. Hijikata, Y. Kubota, Y. Mita, J. Kim, M. Takata and S. Kitagawa, *Nat. Chem.*, 2010, **2**, 633-637.
29. L. J. Li, S. F. Tang, X. X. Lv, X. R. Xu, X. B. Zhao and K. M. Thomas.*To be submitted*.
30. C. Gómez-Navarro, R. T. Weitz, A. M. Bittner, M. Scolari, A. Mews, M. Burghard and K. Kern, *Nano Lett.*, 2007, **7**, 3499-3503.
31. S. J. Guo and S. J. Dong, *Chem. Soc. Rev.*, 2011, **40**, 2644-2672.
32. T. Q. Xu, Q. L. Zhang, J. N. Zheng, Z. Y. Lv, J. Wei, A. J. Wang and J. J. Feng, *Electrochim. Acta*, 2014, **115**, 109-115.
33. J. Liu, J. T. Culp, S. Natesakhawat, B. C. Bockrath, B. Zande, S. G. Sankar, G. Garberoglio and J. K. Johnson, *J. Phys. Chem. C*, 2007, **111**, 9305-9313.
34. A. Domenech, H. Garcia, M. T. Domenech-Carbo and F. X. L. I. Xamena, *J. Phys. Chem. C*, 2007, **111**, 13701-13711.
35. S. Loera-Serna, M. A. Oliver-Tolentino, M. D. Lopez-Nunez, A. Santana-Cruz, A. Guzman-Vargas, R. Cabrera-Sierra, H. I. Beltran and J. Flores, *J. Alloys Compd.*, 2012, **540**, 113-120.
36. Z. Bo, W. Zhu, W. Ma, Z. Wen, X. Shuai, J. Chen, J. Yan, Z. Wang, K. Cen and X. Feng, *Adv. Mater.*, 2013, **25**, 5799-5806.
37. K. Kim, Z. Lee, B. D. Malone, K. T. Chan, B. Aleman, W. Regan, W. Gannett, M. F. Crommie, M. L. Cohen and A. Zettl, *Phys. Rev. B*, 2011, **83**, 245433-245452.
38. Y. Feng, T. He and N. Alonso-Vante, *Electrochim. Acta*, 2009, **54**, 5252-5256.

Graphical abstract

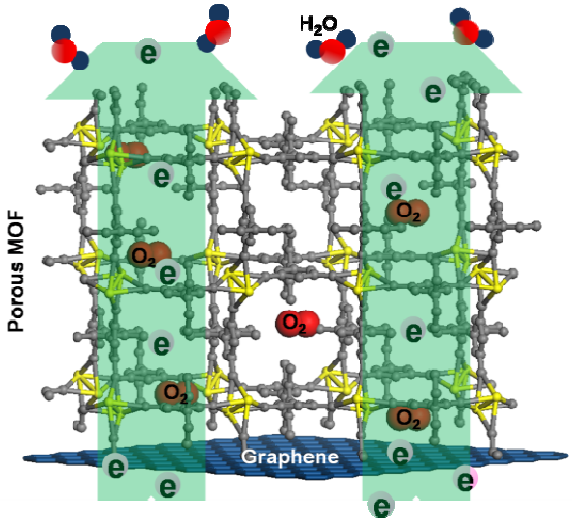

A stable highly porous metal-organic framework (MOF) layer on reduced graphene oxide immobilized glassy carbon electrode performs good electrocatalytic activity for oxygen reduction reaction.